https://doi.org/10.61092/iaea.572h-t615

INDC(NDS)-0886
Distr. G,NM,PH

IAEA
International Atomic Energy Agency

INDC International Nuclear Data Committee

Thermal Neutron Capture in the Low Mass Region

Jiri Kopecky
JUKO Research
Alkmaar, The Netherlands

December 2023

IAEA Nuclear Data Section
Vienna International Centre, P.O. Box 100, 1400 Vienna, Austria

Selected INDC documents may be downloaded in electronic form from
http://nds.iaea.org/publications
or sent as an e-mail attachment.
Requests for hardcopy or e-mail transmittal should be directed to
NDS.Contact-Point@iaea.org
or to:
Nuclear Data Section
International Atomic Energy Agency
Vienna International Centre
PO Box 100
1400 Vienna
Austria

Printed by the IAEA in Austria

December 2023

INDC(NDS)-0886
Distr. G,NM,PH

Thermal Neutron Capture in the Low Mass Region

Jiri Kopecky
JUKO Research
Alkmaar, The Netherlands

December 2023

Contents

1. Introduction

Photon strength functions (PSF) form the basic input information for theoretical models of nuclear reactions and many applications. The increased interest and state of the art of these data are described in detail in Goriely, et al. [1], prepared within the IAEA-NDS Coordinated Research Project which was concluded in 2019. The derived PSF data have been supported theoretically by two recently developed models, the empirical model SMLO [2] and the semi-microscopic model D1M + QRPA [3]. However, one of the major remaining questions from these studies is understanding and validating the behaviour of the PSF as it approaches the limit $E_\gamma \sim 0$, this being especially important for astrophysics applications.

Another important aspect is that the PSF describe the γ-ray decay properties from excitations of nucleonic systems in the statistical condition and that according to the Brink hypothesis, it depends only on the gamma-ray energy and is independent of any other quantity. Any nonstatistical decay mode interfering with the statistical component would cause a violation of this rule because it would strongly depend on the condition of the initial state of the decay.

The Low Energy Enhancement (LEE) was first observed in the OSLO experiments in 2005 [4,5] as well as in many following measurements. To add this LEE component to existing models, a 0lim prescription based on phenomenological studies [6] has been added to the existing SLMO and D1M + QRPA models with the working name "upbend". The free parameters of the global formulae for E1 and M1 radiation have been adjusted to Shell-Model results and to available low-energy data from the Oslo method.

As a general observation, there is no global neutron capture model that is valid for all masses and incident excitation regions. Consequently, the various excitation regions (low, medium, and high) must be considered separately, as was clearly demonstrated in Ref. [7] which focused on the validation of PSF data obtained from different experimental techniques (see Figs 3 and 4 therein). Following these conclusions, a separate study of different mass regions was undertaken to disentangle the energy and mass dependent effects of the different models. In the present work, we address the low mass region with $A < 70$, where thermal capture is dominant and due to excellent spectroscopic results, the transition multipolarities can be determined. The latter is a crucial factor for separating the E1 from the M1 data and for further extending the E_γ limit close to zero energy. Other capture techniques, such as DRC or ARC, are suitable for studying larger masses with $A > 70$ as they feature averaging over many resonances and hence decrease the influence of the PT fluctuations. However, as a downside, experimental data are extremely scarce below $E_\gamma \sim 3$ MeV. This makes the thermal capture method unique for studying experimental PSF data in the 0lim region and worth revisiting and reanalysing to gain deeper insight into the behaviour of the PSF in the low energy limit.

2. Update of the thermal A < 70 PSF data

Thermal capture PSF data have been studied in detail in Refs [8,9]. Data for 30 nuclides in the medium mass region ($A < 160$), from ^{20}F up to ^{154}Eu, were processed in the database *'IAEA PSF database 19 Sep 2022'* (*https://www-nds.iaea.org/PSFdatabase/*). Nuclides with masses below $A \sim 70$ have been reviewed for the presence of non-statistical contributions using both the (n,γ)(d,p) linear correlations and the slope analysis (see sections 2.1 – 2.6 in Ref. [9]). All stable nuclides with reliable capture data were considered and only two of them (^{20}Ne and ^{47}Ti) were excluded. A complete and extended database of PSF has been thus produced in this mass

region. The present work has further updated the thermal database with additions and/or replacements in the mass region A ≤ 70 as listed in Table 1. The recent thermal capture PSF database has also been extended by adding newly available data between A = 7 and A = 70 to build a complete set of data for relevant stable nuclides.

The update primarily includes results from several dedicated laboratories, which in chronological order are the ECN Petten, the UJF Rez/TU Munich, the latest Oak Ridge/Los Alamos (LANL/ORNL) and the very recent IRK Budapest/UJF Rez collaborations. A common feature of these data is the high quality of the derived decay schemes based on the absolute transitions' intensity calibration. Especially the latest entry of ^{57}Fe [10] clearly demonstrates the high quality of these recent measurements and will be discussed in detail.

TABLE 1. Listing of neutron capture measurements for light nuclides (A < 70) with final recommendations. The list includes data for 50 nuclides in the 7 ≤ A ≤ 70 mass range, including new entries and all the new recommendations, which are shown in the last two columns. Data denoted as EGAF have been extracted from the EGAF section of the IAEA NDS PGAA database.

Used notations:

x	included in both database versions
X	recommended data as the best choice
0	data considered only for the DC analysis and rejected for the PSF determination either because of the limited number of transitions (<5) or because E_γ data were available in a narrow region above 5 MeV (^{67}Zn)
EGAF	partial data extracted from the IAEA NDS PGAA database.

-[19 Sep 2022]-				[30 June 2023] additions/replacements-			
Product	**THC**	**EGAF**		**THC**	**PSF**	**New entry / Laboratory**	**Ref.**
Li-7				X	0	LosAlamos/OakRidge	[11]
C-12				X	0	BNL	[12]
C-13				X	0	BNL	[12]
N-15				**X**	x	LosAlamos/OakRidge	[13]
O-18				X	0		
F-20	**X**				x		
Ne-21				**X**	x	McMaster	[14]
Na-24	x			**X**	x	UJF Rez/TU Munich	[15]
Mg-25	**X**				x		
Mg-26	**X**	x			x		
Mg-27				**X**	x	LosAlamos/OakRidge	[16]
Al-28	**X**				x		
Si-29	**X**				x		
Si-30	x	**X**			x		
Si-31				**X**	x	LosAlamos/OakRidge	[17]
P-32	**X**				x		
S-33	x	x		**X**	x	LosAlamos/OakRidge	[18]
S-34	x	x		**X**	x	LosAlamos/OakRidge	[18]
S-35	x			**X**	x	LosAlamos /OakRidge	[18]
S-37				**X**	x	LosAlamos/OakRidge	[19]
Cl-36	X				x		
Cl-38	**X**				x		
Ar-41	x	**X**			x		
K-40	**X**				x		
K-41	x	**X**			x		
K-42	x	**X**			x		
Ca-41	**X**				x		
Ca-43	x	**X**			x		
Ca-44	x	**X**			x		
Ca-45	x	**X**			x		
Sc-46	**X**				x		
Ti-48				**X**	x	ECN Petten	[20]
Ti-49	x			**X**	x	ECN Petten	[20]
Ti-50	x	x		**X**	x	ECN Petten	[20]
Ti-51					x		
V-51		**X**			x		
V-52		**X**			x		
Cr-51	x	**X**			x	EGAF	
Cr-53				**X**	x	DRC + EGAF	
Cr-54				X	x	EGAF	
Cr-55				**X**	x	EGAF	
Mn-56		**X**			x		
Fe-55				**X**	x	ECN Petten	[21]
Fe-57	x				x	IKP Budapest/UJF Rez	[10]
Fe-58	**X**				x		
Fe-59		**X**			x		
Co-60	**X**	**X**			x		
Ni-59	x	x		**X**	x	LosAlamos/OakRidge	[22]
Ni-60				**X**	x	LosAlamos/OakRidge	[22]
Ni-61	x			**X**	x	LosAlamos/OakRidge	[22]
Ni-63	x	**X**			x		
Ni-65		**X**			x		
Cu-64	**X**				x		
Cu-66	**X**				x		
Zn-65	**X**				x		
Zn-67				x	0	EGAF	
Zn-68	**X**				x		
Zn-69				**X**	x	EGAF	

The list of re-analyzed and/or new entries added to the previous *'IAEA PSF database 19 Sep 2022'* (*https://www-nds.iaea.org/PSFdatabase/*) includes the following nuclides: ^{7}Li, ^{12,13}C, ^{15}N, ^{18}O, ^{21}Ne, ^{24}Na, ^{27}Mg,^{31}Si, ^{33,34,35,37}S, ^{48,49,506}Ti, ^{51,53,54,55}Cr, ^{55,57,59}Fe, ^{59,60,61}Ni and ^{67,69}Zn. The included data are in the standard PSF format and form a complete list of important stable nuclides for masses below A ~ 70.

3. The nonstatistical model in neutron capture

3.1. E1 direct capture in the A < 70 region

The first model of Direct Capture (DC) for E1 transitions was introduced by Lane and Lynn in 1960 [23] and was successfully applied to light mass targets in the $3s_{1/2} - 2p_{1/2,3/2}$ single particle region with mass A < 62. The thermal E1 capture data are thus based on two model components, the statistical compound nucleus model and the nonstatistical DC component. Recently, the DC option has been included in the latest version of the TALYS code [24].

Several aspects of the Lane-Lynn model have been developed since its conception, such as introducing a different power of E_γ for the transition from the expected single-particle E_γ^3. This different dependence on E_γ was noticed by the RCN Petten group when studying correlations between I_γ^3 and $(2J_f + 1)S_f$ values from the (n,γ) and (d,p) reactions, respectively (see Refs [25-27]). This feature of differing dependence on E_γ has become an important tool to investigate the reaction mechanism and has led to the introduction of direct capture in the hard-sphere and resonance (valence) components of the reaction which interfere coherently. The influence from these correlations resulted in the revision of the E_γ dependence of the DRC model by Lane in 1974 as described in Ref. [28]. The photon energy dependence varies according to the relative contributions of the two mechanisms, direct and statistical, as ~ E_γ^1, ~E_γ^2 and approaches E_γ^5 when the statistical contributions become non-negligible. This gradual modification of the formula for different mass and neutron energy regions was discussed in detail by Kopecky in [9] and the consequences were demonstrated in the historical Fig. 1 taken from the study of (d,p)(n,γ) correlation in Ref. [29].

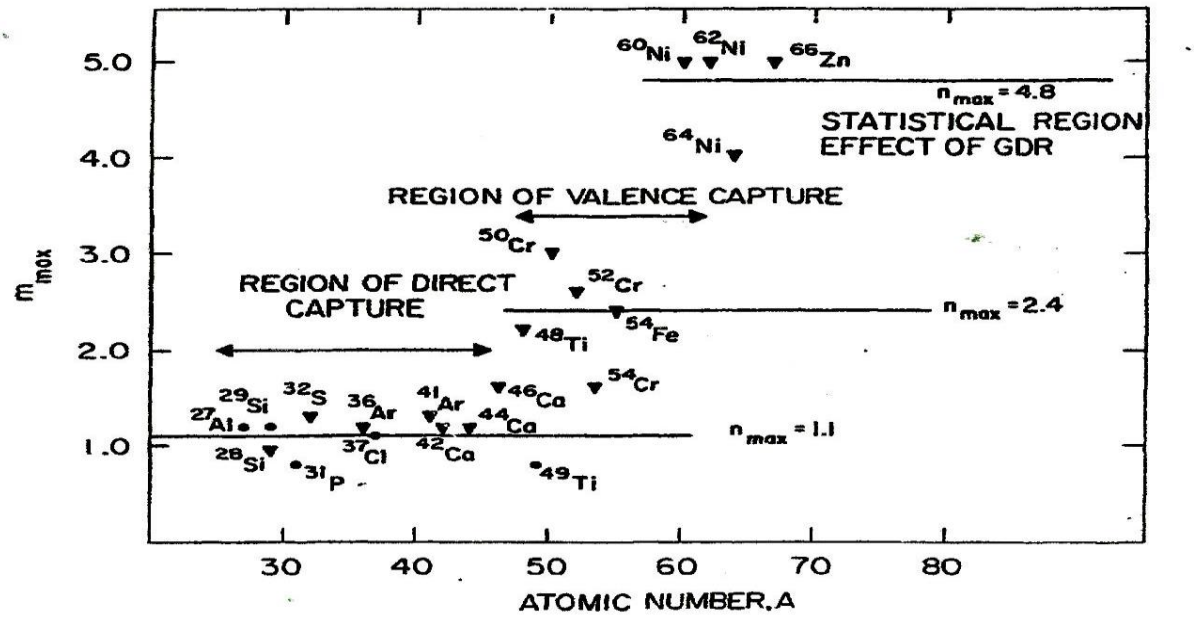

FIG. 1. taken from Ref. [29]. *Variation of the n_{max} of the reduced energy E_γ^n with mass A deduced the (n,g)(d,p) correlations method introduced by NRG Petten group in Refs [25,26,27]. The data are separated in three groups associated with three different capture modes, the DRC, valence and "doorway state" in the statistical componen region. Note that this figure displays the picture from 1978.*

The correlation analysis was an indirect signature of the presence of DC till Mughabghab published the first quantitative verification of the presence of direct capture, showing an exceptional agreement between the calculated and experimental E1 primary cross sections in the $^{136}Xe(n,\gamma)^{137}Xe$ reaction, in 1979 [29]. The effort in this field continued with the publication of the BNL cross-section books [31] which included the $\sigma_i(D)$ partial E1 cross sections for many nuclides in the mass region $7 < A < 200$ in the resonance parameters input, for those cases where the s → p transitions dominated the decay scheme. The total DC values were obtained from $\sigma(D) = \Sigma^i\sigma_i(D)$, however, without information on parameters used (the scattering lengths or S_{dp}) and the assigned E1 transitions. The accuracy of such a calculation depends significantly on these assignments. As no $\sigma(D)$ uncertainty is provided in Ref. [31], an uncertainty of 50% is assumed in the present analysis.

Since 1985, the DRC theory has been developed and new measurements have been performed by Lynn and Raman [11,17,18,19,22]. The mechanism by which the captured neutron is transferred from the direct (D) via valence (V) into the statistical capture (CN) has been formulated in detail and applied in the analysis of the new measurements. The main difference between Mughabghab's [31] and Lynn's formulation is in the treatment of the interference term between statistical $\sigma(CN)$ and non-statistical $\sigma(D)$ components. In Mughabghab's approach, the interference term is either absent or negligible, while Lynn and Raman [30] consider the sum of amplitudes according to equation $\sigma(\text{exp}) = (\sqrt{\sigma(D)} \pm \sqrt{\sigma(CN)})^2$.

In the present analysis, the total $\sigma(D)$ value has been, after first checking the E1 assignments, obtained from the calculated $\sigma_i(D)$, using $\sigma(D) = \Sigma^i\sigma_i(D)$ (as is shown in Section 3.2., Table 3) and included in the final analysis.

3.2. Comparison of the DRC E1 calculations

The comparison of partial experimental and theoretical DC predictions has been the subject of several publications and presentations. However, a systematic study of the DC contribution of the E1 thermal capture cross section has yet to be done. Calculated total DC cross sections, obtained by using the formalism of the "simple direct process" for E1 transitions of Ref. [23], have been included in all BNL thermal cross-section book series from 1984 to 2018 [31]. The results of these calculations have been compiled along with experimental cross sections, and other components such as the positive energy resonances, the negative energy contributions called σ(B) non-resonant bound contributions, and the non-statistical calculated values denoted as σ(D). In all these calculations, it has been assumed that the interference term between the D and resonance (CN) components is absent or negligible. It must be noted that all these cross sections, except σ(D), include the total detected gamma ray (E1+M1+E2) strength.

To quantify the DC contributions, the calculated σ(D) must be associated with the total E1 strength and the absolute primary I_γ intensities. Note here that the deexcitation of the capture state must be close to unity. In such a case, one can be sure that the decay scheme is complete, and most of the strength is considered. Furthermore, the spin and most importantly, the parity of the final states needs to be known to assign the multipolarity of the transition. The corresponding total E1 strength is then calculated from the $\sigma(E1) = \sigma_\gamma \Sigma I_\gamma(E1)$ equation using the total thermal cross section σ_γ. The uncertainty of σ(E1) is heavily influenced by the quality of the absolute normalization of the intensity I_γ and by the E1 and M1 assignments that should be based on strong parity arguments. The presence of Porter-Thomas fluctuations prevents making any reliable intensity assignments. Transitions to states with no parity assignments should not be considered. Results of the analysis of the strengths of both E1 and M1 transitions depopulating the capture state are given in Table 2. An important conclusion can be drawn from Table 2 concerning the E1/ M1 strength ratio over the whole E_γ range. This ratio confirms the expected dominance of the E1 strength in the 3s– $2p_{1/2/3/2}$ shell region as can be seen in Fig. 2 and Table 2 with E1 and M1 being components of the total capture cross section σ_γ.

TABLE 2. The σ(E1) and σ(M1) contributions for light mass targets. All cross sections are in barns. All $\sigma(g)_0$ values above 1.5 b (arbitrarily chosen) are printed in red as they are cases with a dominant resonance capture and corresponding effects.

Used notations:

σ_γ	Thermal cross section taken from the BNL cross section book [31]
ΣIgE1,M1	Total E1 and M1 strength
no Jpi	Transitions to states with no parity assignment or missing de-excitation
σ(E1)σ(M1)	E1 and M1 total cross sections
E1/M1	The ratio of the E1 and M1 strengths

Nuclide		σγ	ΣIgE1	ΣIgM1	no Jpi	σ(E1)	σ(M1)	E1/M1
Li	7	0.0445	1			0.045		
C	13	0.00387	0.998	0.16		0.004	0.001	6.5
	14	0.0015	0.925	0.074		0.001	0.000	9.0
N	15	0.080	0.43	0.57		0.034	0.046	0.7
O	18	0.00054	0.99	0.01		0.00053	0.00007	99.0
F	20	0.0095	0.6	0.4		0.006	0.004	1.6
Ne	21	0.039	0.75	0.032		0.029	0.001	23.2
Na	24	0.525	0.42	0.59		0.221	0.310	0.7
Mg	25	0.0538	0.52	0.49		0.028	0.026	1.1
	26	0.199	0.2	0.84		0.040	0.167	0.2
	27	0.0374	0.32	0.7		0.012	0.026	0.5
Al	28	0.231	0.48	0.53		0.111	0.122	0.9
Si	29	0.177	0.9	0.1		0.159	0.018	9.0
	30	0.119	0.75	0.25		0.089	0.030	3.0
	31	0.107	0.98	0.02		0.105	0.002	49.1
P	32	0.166	0.63	0.35		0.105	0.058	1.8
S	33	0.518	0.94	0.069		0.487	0.036	13.6
	34	0.454	0.41	0.59		0.186	0.268	0.7
	35	0.256	0.92	0.04		0.236	0.010	23.0
	37	0.236	1			0.236		
Cl	36	43.6	0.49	0.45		21.364	19.620	1.1
	38	0.433	0.92			0.398		
Ar	41	0.66	0.99	0.01		0.653	0.007	98.9
K	40	2.1	0.48	0.53		1.008	1.113	0.9
	41	38.8	0.63	0.29	0.08	24.444	11.252	2.2
	42	1.46	0.79	0.15	0.06	1.153	0.219	5.3
Ca	41	0.41	0.82	0.05		0.336	0.021	16.4
	43	0.68	0.99	0.01		0.675	0.005	141.8
	44	6.2	0.82	0.12	0.06	5.102	0.750	6.8
	45	0.88	0.45	0.55		0.396	0.486	0.8
	47	0.74	0.96	0.04		0.707	0.033	21.7
	49	1.09	1			1.090		
Sc	46	27.2	0.42	0.37		11.424	10.064	1.1
Ti	49	8.32	0.98	0.02		8.154	0.166	49.0
	50	1.87	0.98	0.01		1.833	0.019	98.0
V	51	45	0.661	0.035	0.305	29.745	1.575	18.9
	52	4.94	0.92	0.035		4.545	0.173	26.3
Cr	51	14.7	0.86			12.642		
	53	0.86	0.83			0.714		
	54	18.6	0.95	0.05		17.670		
Mn	56	13.36	0.82	0.18		10.955	2.405	4.6
Fe	55	2.3	0.94		0.03	2.160		
	57	2.59	0.48	0.53		1.243	1.373	0.9
	58	2.48	0.93			2.306		

	59	1.32	0.89	0.03	0.08	1.175	0.040	29.7
Co	60	37.18	0.76	0.02		28.257	0.744	38.0
Ni	59	4.39	1.00	0.00		4.386	0.004	999.1
	60	73.7	0.78	0.01	0.078	57.486	0.737	78.0
	61	2.45	0.98	0.01	0.008	2.401	0.021	112.6
	63	14.9	0.78	0.12	0.096	11.662	1.803	6.5
	65	1.63	0.98	0.01	0.003	1.603	0.022	73.9
Cu	64	4.5	0.8	0.02		3.600	0.090	40.0
	66	2.17	0.72	0.09		1.562	0.195	8.0
Zn	65	0.731	0.95	0.05		0.694	0.037	19.0
	67	0.62	0.97			0.601		
	68	7.5	0.92	0.08		6.900	0.600	11.5
	69	1.07	0.67	0.33		0.717	0.353	2.0

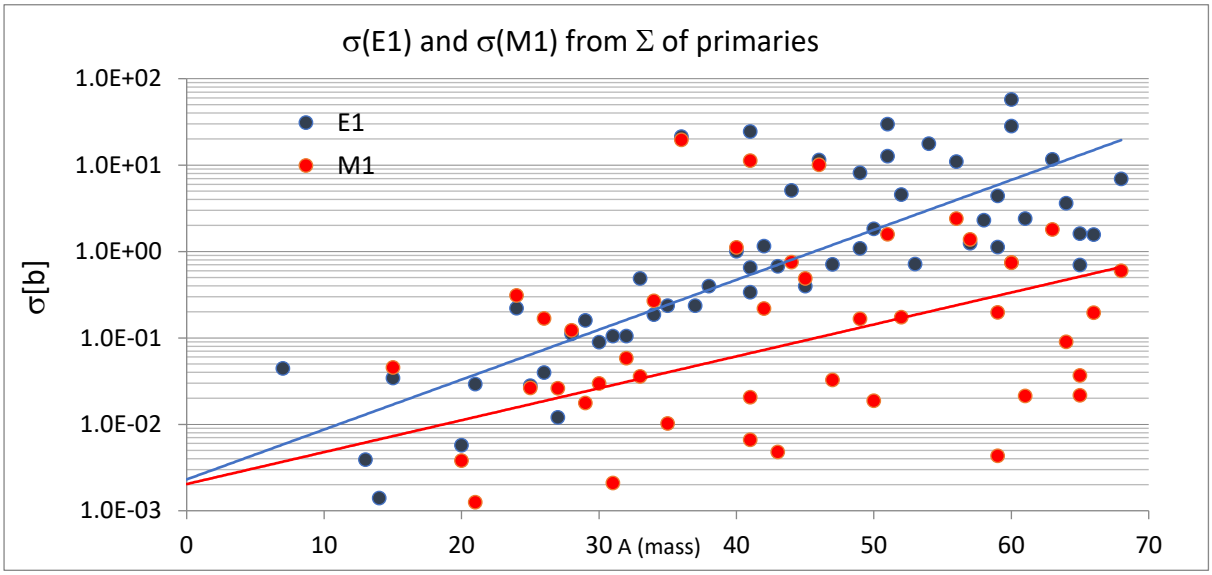

FIG. 2. *The E1 and M1 fractions of the total thermal capture cross sections based on assigned E1 and M1 primary intensities of the capture state deexcitation. Note that cross sections below A ~ 40 are all, except ^{36}Cl, smaller than 1 b, which suggests the off-resonant origin of the capture. The resonant contribution above A ~ 40 becomes important with increasing mass.*

Most of the data for A < 40 have σ_γ smaller than 1b and are typical off-resonant capture data. Higher thermal cross-sections (above ~ 1.5 b) indicate the presence of resonance contributions and are shown in Table 2 as red σ_γ values. The E1/M1 ratio confirms the expected dominance of the E1 strength in the $3s_{1/2} - 2p_{1/2/3/2}$ shell region but shows a rather dynamic behavior. The E1/M1values range from being strongly dominated by E1 strength to competing E1 and M1 strengths. The total σ(E1) results can also be compared with the calculated DRC predictions to show the relative contribution of the DRC to the total E1 strength. The results of this analysis are shown in Table 3.

TABLE 3. Results of nonstatistical σ(E1) contributions for light mass targets. All cross sections are given in barns, the red printed cross section $\sigma(\gamma)_0$ values suggest again the presence of a strong resonance capture.

Used notations:

σ_γ	Thermal cross section taken from Ref. [30]
σ(E1)	Total E1 and M1 strength ΣIgE1 converted in σ(E1)
σ(D)	Calculated total cross sections from BNL Ref. [30] or Los Alamos (LANL/ORNL) data; a sum of partial DC data from Refs [11-22]
σ (D)/σ(E1)	The ratio to the calculated/measured E1 total cross sections

				BNL		LA + ORNL	
Nuclide		**σγ**	**σ(E1)**	**σ(D)**	**σ(D)/σ(E1)**	**σ(D)**	**σ(D)/σ(E1)**
Li	7	0.0445	0.0445	0.052	1.16		
C	13	0.0039	0.0039	0.0035	0.91	0.0034	0.87
	14	0.0015	0.0014	0.0014	0.98	0.0012	0.82
N	15	0.080	0.0344			0.022	0.64
O	18	0.0005	0.0005	0.0005	1.00		
F	20	0.0095	0.0057	0.0047	0.82	0.0042	0.74
Ne	21	0.039	0.0293	0.0382	1.30		
Na	24	0.525	0.2205	0.057	0.26	0.0303	0.14
Mg	25	0.0538	0.028	0.013	0.46	0.0241	0.86
	26	0.199	0.0398			0.0368	0.92
	27	0.0374	0.012	0.037	3.08	0.0452	3.77
Al	28	0.231	0.1109	0.108	0.97		
Si	29	0.177	0.1593	0.132	0.83	0.133	0.83
	30	0.119	0.0893	0.078	0.87	0.064	0.72
	31	0.107	0.1049	0.081	0.77	0.084	0.80
P	32	0.166	0.1046	0.11	1.05	0.105	1.00
S	33	0.518	0.4869	0.401	0.82	0.412	0.85
	34	0.454	0.1861	0.157	0.84	0.18	0.97
	35	0.256	0.2355	0.224	0.95	0.231	0.98
	37	0.236	0.236			0.211	0.89
Cl	36	43.6	21.364				
	38	0.433	0.3984	0.4	1.00		
Ar	41	0.66	0.6534	0.514	0.79		
K	40	2.1	1.008	0.753	0.75		
	41	38.8	24.444				
	42	1.46	1.1534	1.32	1.14		
Ca	41	0.41	0.3362	0.23	0.68	0.355	1.06
	43	0.68	0.6752	0.68	1.01	0.670	0.99
	44	6.2	5.102			2.30	0.37
3	45	0.88	0.396	0.865	2.18	1.284	3.24
	47	0.74	0.7074			0.536	0.78
	49	1.09	1.09	1.09	1.00	1.463	1.34
Sc	46	27.2	11.424				
Ti	49	8.32	8.1536	8.18	1.00		

	50	1.87	1.8326	2.01	1.10		
V	51	45	29.745				
	52	4.94	4.5448				
Cr	51	14.7	12.642	9.6	0.76		
	53	0.86	0.7138	0.31	0.43		
	54	18.6	17.67	17.8	1.01		
Mn	56	13.36	10.955				
Fe	55	2.3	2.16	0.98	0.46		
	57	2.59	1.2432	0.97	0.78		
	58	2.48	2.3064	0.55	0.24		
	59	1.32	1.122	1.74	1.55		
Co	60	37.18	28.257				
Ni	59	4.39	4.3856	4.11	0.94	6.762	1.54
	60	73.7	57.486				
	61	2.45	2.401	1.09	0.45	1.252	0.52
	63	14.9	11.6622	9.05	0.78		
	65	1.63	1.6029	1.37	0.85		
Cu	64	4.5	3.6				
	66	2.17	1.5624				
Zn	65	0.731	0.6945	0.155	0.54		
	67	0.62	0.6	0.05	0.08		
	68	7.5	6.9				
	69	1.07	0.72	0.006	0.01		

Comparison of the predicted (calculated) DC strength with the experimentally extracted total E1 strength is shown in two columns denoted '$\sigma(D)/\sigma(g)$' in Table 3 using two independent calculations from the BNL and LANL/ORNL collaboration (see the text above).

Remarks on Table 3:

1. The BNL calculations from Ref. [31] are robust, for all potential direct-capture candidates in the light mass region below A ~ 70, the (4s – 3p) region with masses 130 < A <150 and finally in the closed shell Pb region. The two latter regions are mentioned here only for completeness but are not discussed further. The BNL results, however, have been provided without any information on the parameters that were used in the calculation or the adopted E1 transitions. The quoted σ(D) value is a sum of partial data of all E1 transitions.
2. The LANL/ORNL partial transition data were extracted from Refs [11-22] and summed to obtain the total σ(D) for the present study. Knowledge of the assigned E1 transitions allowed us to compare with the recent final state spin and parity values from the ENDSF database. As a result, several questionable cases were spotted (such as ^{59}Ni) and corrected in the total σ(D) values.

The results of the comparison are shown in Figs 3 and 4. All available data are shown in Fig. 3 including the outliers. The fitted curves are exponential trend fits to the mass A. The data qualifying as outliers have σ(D)/σ(E1) values different by factors of 3 or more from unity. Several sources contribute to the uncertainty budget of the ratio, including a conservative approach to the final value with a fictitious uncertainty factor of ~ 2. Other sources of uncertainty are the uncertainty of σ(E1) which is mainly affected by the E1 transition

assignments, the completeness of the initial state de-excitation, and the absolute normalization of the capture I_γ intensities. The uncertainty of σ(g)o is negligible in this analysis. The main sources of uncertainties for the DRC calculations are the choice of E1 transitions and the knowledge of the spin J_f in the spectroscopic factor $(2J_f + 1)S_n$ of the (d,p) strength used in the DRC formula.

Among the larger outliers are the ^{24}Na, ^{27}Mg and ^{45}Ca nuclides. Several minor corrections of the E1 transition assignments have been implemented (as for ^{59}Ni) but with relatively small impact on the σ(E1) value.

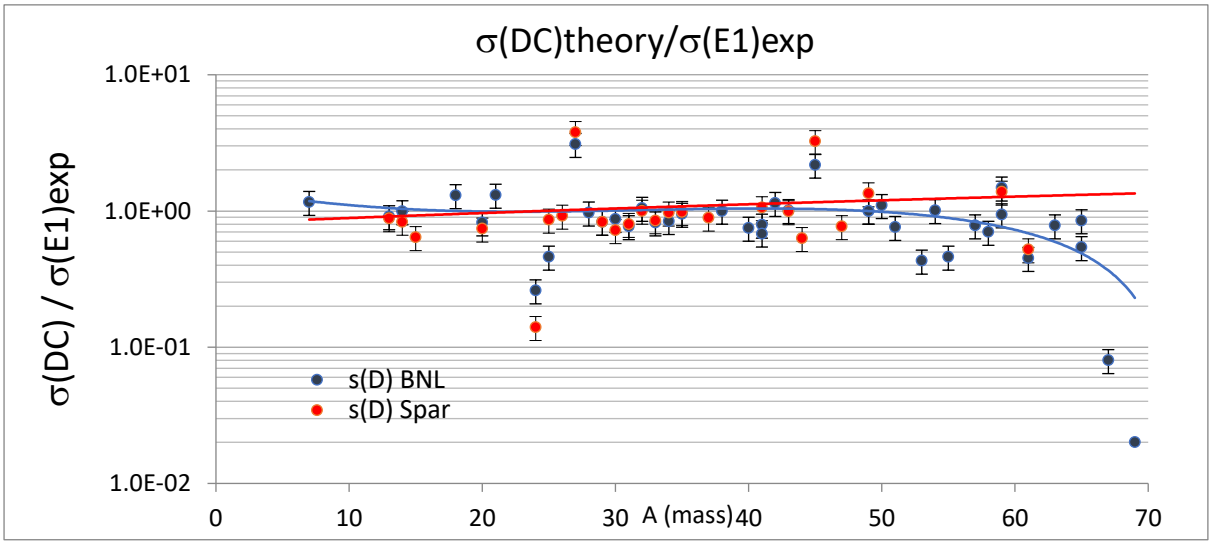

FIG. 3. *The ratio of the calculated and experimental DC total strength for E1 radiation plotted as a function of the mass A. The blues points belong to the BNL results and the red ones to the Los Alamos Oak Ridge collaboration (the sum of partial data Σpar). Note that the ratio data are close to one which indicates the dominance of the DC in the E1 strength in the whole energy region. Three data pairs, considered as the outliers, are discussed further. The fitted dependence are the trend exponential curves as a function of A. Note the sharp and expected decrease of the DC component in the Zn isotopes.*

The results for the following nuclides, ^{24}Na, ^{27}Mg, and ^{45}Ca merit further discussion. All three nuclides have a sizeable contribution from M1 transitions. The calculated values from both above-mentioned independent approaches (1) and (2) have a similar feature, namely a strong competition between E1 and M1 strengths. The uncertainty of the total σ_γ is negligible, probably smaller than 10%. Since the E1 and M1 transitions used in both calculations were difficult to trace, it was decided to omit these data from the analysis and the results are shown in Fig. 4.

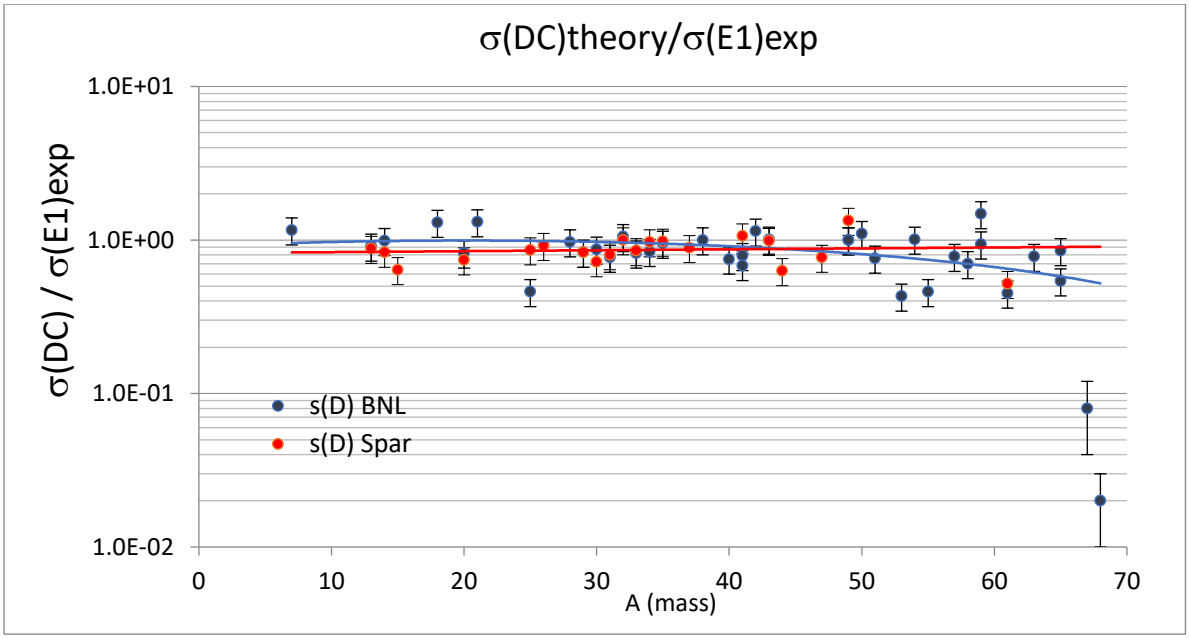

FIG. 4. *The ratio of the calculated and experimental DC total strength for E1 transitions plotted as a function of the mass A. The estimated associated 20% uncertainty is included. The blue points belong to the BNL results and the red ones to the Los Alamos/Oak Ridge collaboration (the sum of partial σ(D) data). The outlying data have been either corrected (for incorrect E1 assignments) or removed (*^{24}Na, ^{27}Mg, and ^{45}Ca*). Note that the DC strength is close to the total E1 strength up to Zn isotopes. The fitted dependence are the eye guiding trend curves as a function of A.*

It is difficult to estimate the uncertainty of the calculated ratios. It reflects primarily the goodness of the agreement between the E1 transition assignments involved in σ(E1) and those considered in the calculations. The calculations are further afflicted by the uncertainties of the final state spins in the term (d,p) $(2J_f+1)S_n$ depending on whether $J_f = J_i \pm 1/2$ or 3/2 was used. Since the final state spin is uniquely determined for the major transitions, we have adopted a conservative estimate for these two uncertainty sources.

E1 Conclusions: The dominance of DC for the low-mass A < 70 region is demonstrated in Fig. 4. Both calculations predict the DC E1 strength depopulation of the initial state to be about 80 to 100 % confirming that the E1 strength dominates the LEE component below 3 MeV. An attempt to determine the statistical compound nucleus (CN) tail contribution by LANL/ORNL has resulted in large uncertainties. To summarize:

- The theoretical formula describing the total E1 strength in the whole energy range and for masses A < 70, is a combination of nonstatistical contributions, among which the DRC is dominant, and the statistical GDR(E1) contribution. The DRC model explains the LEE E1 behavior in this mass region for thermal capture.
- The relative contribution of DC is related to the specific composition of the thermal capture state. With incerasing neutron energy, it also depends on the purely resonance capture (DRC and ARC) components, as the statistical behavior of the compound hard core becomes dominant and the influence of the DC starts to diminish. This means that thermal capture PSF data may differ from the general PSF values depending on the relative contribution of the statistical decay of the initial capture states below the B_n values.
- The E1/M1 strength ratio can be used to validate the upbend systematics [6] for nuclides with masses A < 70.

3.3. M1 capture

The primary M1 strength was not consistently addressed during the development of the Direct Capture Theory in the seventies, probably due to its relatively small contribution to thermal cross sections and in many cases due to the lack of low-energy transitions. Both features result from a combination of experimental limitations and nuclear structure effects that suppress M1 transitions, especially for nuclei with A > 46. A notable exception is the ^{57}Fe nucleus, where both experimental data and low-energy M1 transitions are strongly present. The relative M1 strength as a function of the mass A and energy E_γ is shown in Figs 5 and 6.

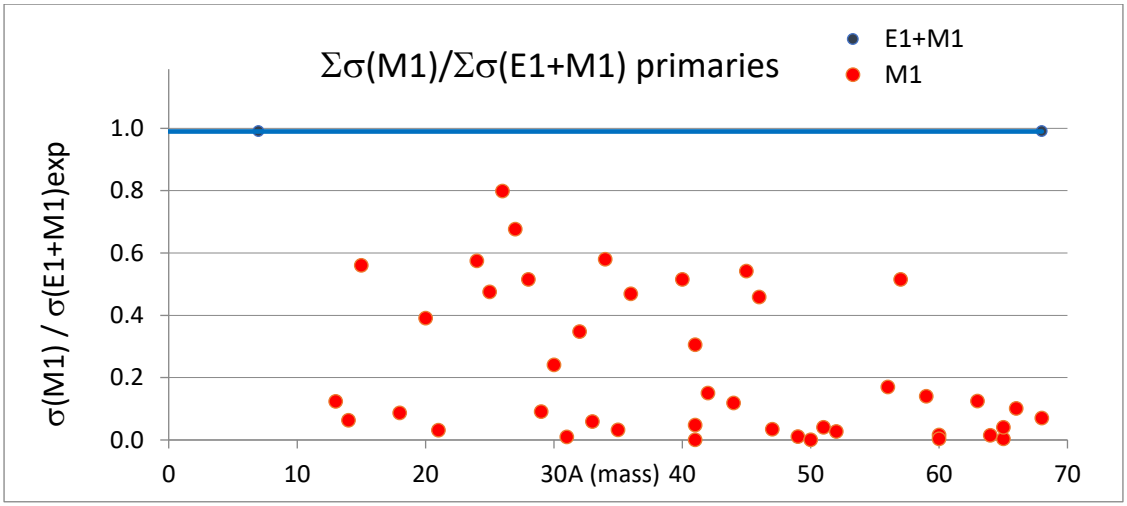

FIG. 5. *The ratio of the M1 radiation to the total absolute primary strength (E1+M1) taken from Table 2. Note that comparable M1 strength is present only for nuclei below ^{46}Sc and becomes negligible for heavier nuclides except for ^{57}Fe. This is mainly due to the limited availability of suitable final states.*

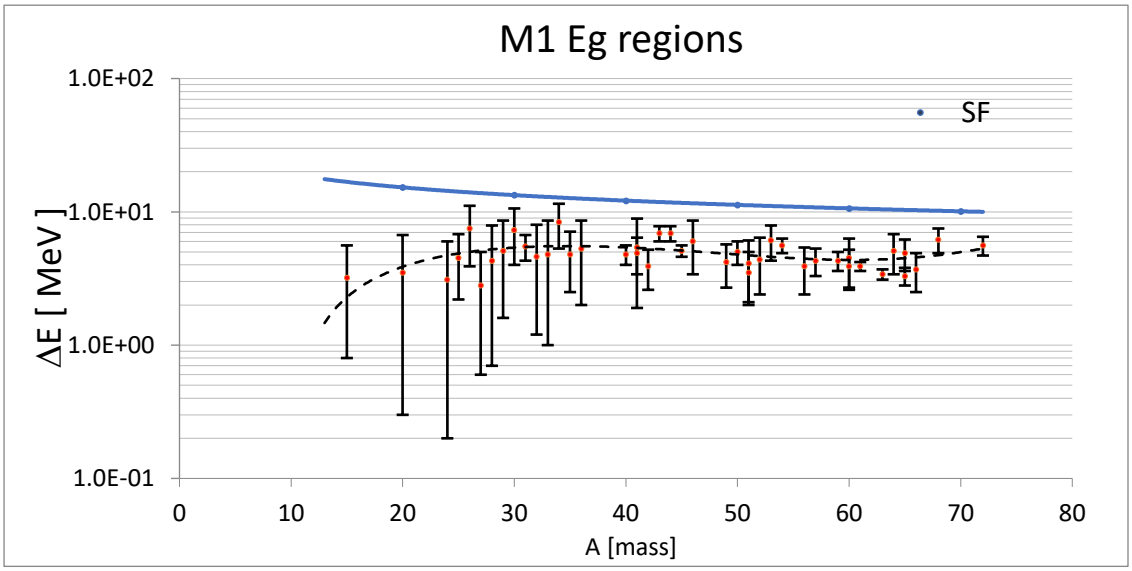

FIG. 6. *The energy region ΔE between the lowest and highest M1 transition as a function of mass A. The dotted curve represents the unweighted polynomial trend line of the middle energy of the M1 energy window serving as an eye guide. The blue curve follows the spin-flip (SF) energy E_o prediction and influences the M1 strength for A > 40 nuclides. Note that data for nuclides with A > 40 are all above 3 MeV.*

The direct M1 process is forbidden under the single particle model (SPM) assumptions for $3s_{1/2}$ -> $2s_{1/2}$ transitions. Bohr and Mottelson proposed an M1 giant Lorentzian resonance with the spin-flip mechanism (SF) to account for the observed enhancement of M1 radiation over the Weisskopf SP prediction [32]. The M1 strength distribution is expected to be statistical in nature and the SF resonance energy E_o is predicted to depend on the mass as $E_o = 41\ A^{-1/3}$ MeV. For light nuclides E_o lies above the neutron binding energy and only its tail contributes to the thermal capture. This prediction, however, contradicts the experimental results obtained for nuclides with $A < 40$, where many enhanced M1 transitions have been observed with $E_\gamma \rightarrow 0$. Such behavior suggests the contribution of another process in addition to the statistical SF resonance.

None of the non-statistical effects, so strongly present in E1 capture, were expected to be observed in M1 transitions. It was therefore quite surprising that Kopecky [33] observed a (nγ)(dp) positive correlation for M1 transitions to $l_n = 0$ but not to $l_n = 2$ orbitals, which is a typical signature of the non-statistical process. This surprising observation was further supported by the non-statistical behavior of M1 transitions in the capture spectra from two neighboring s- and p-wave resonances in the ^{35}Cl target [34]. This was the strongest example of the non-conformance of the thermal and resonance capture with the multipolarity rules. The results of the correlation analysis from the late seventies [26, 33, 34] are shown in Table 4.

TABLE 4. The linear correlation coefficient $\rho(I_\gamma/E_\gamma^3, S_{dp})$ of reduced M1 transition strength against the (d,p) spectroscopic factors for a limited number of light nuclides. Note the concentration of the positive correlation for data with $25 < A < 35$. N_f is the number of used transitions.

Target	N_f	σ(M1)	$\rho(I_\gamma/E_\gamma^3, S_{dp})$		
			[32]	[26]	[33]
F-19	6	0.4	-0.17		
Ne-21		0.04			-0.28
Na-23	7	0.59	-0.06		
Mg-25	5	0.49	0.75	0.88	
Al-27	14	0.53	0.78	0.93	
Si-29	4	0.10	0.92		
P-31	5	0.35	0.84		
Cl-35	5	0.49	0.94	1.00	
K-39	3	0.53	0.19		
Fe-56		0.53			-0.08
Fe-57		0.01			0.07
Co-59		0.02			-0.12
Cu-63		0.03			0.02
Ga-71		0.01			-0.02

The theoretical explanation was proposed by Clement and Lane [35] in the form of contribution from a pre-compound semi-direct capture mechanism. The incident s-wave neutron excites the giant M1 resonance (energy E_{M1} rather close to ~ B_n) which under certain conditions emits gamma-rays to s- or d-wave states prior to the statistical decay. This process is similar to the E1 semi-direct model of G.E. Brown from 1964 [36]. Since the s-s(d) capture is forbidden, a process was proposed for target nuclei with a collective M1 giant resonance [34]. Mughabghab speculated that the energy and/or the width of the M1 resonance was smaller and consequently the energy dependence would be faster than $E\gamma^5$ [29].

Lane [37] pointed out that strong initial correlations in nuclei, where resonances are strongly involved, can arise from the semidirect process as well, thus correlation effects may be preserved and consequently lead to the observed non-statistical behaviour of the M1 transition. Clement tested the proposed formalism by calculating the contribution in the case of ^{29}Si to be σ(M1) ~ 130 mb, which fails to explain the data in Table 5 deduced from experimental E1 and M1 parameters by an order of magnitude. The use of E_o(SF) = 7.5 MeV and Γ = 2 MeV parameters

may have been the reason. Kopecky later extended this analysis to masses up to A ~ 130 and presented the results at the Berkeley Conference in 1980 [38,39]. The results are summarized in Fig. 7. The limited number of targets used in the analysis, however, makes it difficult to draw any meaningful conclusion over a broad mass region. To our knowledge, this was the last comprehensive work of this kind on the M1 enhanced strength using the correlation analysis as the signature of the nonstatistical importance of the M1 strength decay.

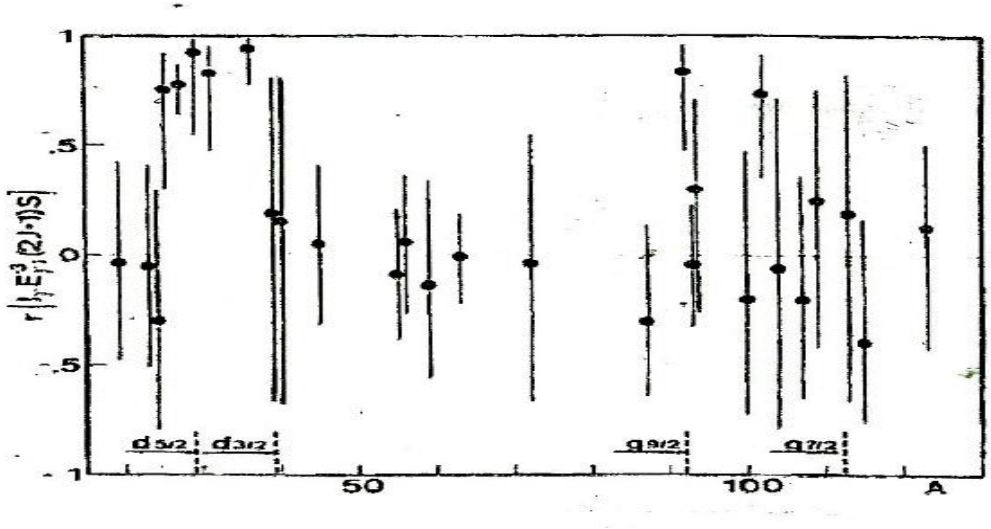

FIG. 7. taken from [37] *Linear correlation coefficients plotted as a function of A. Error bars represent rms errors based on Fisher's 99.9% test. For a detailed discussion of this figure and the explanation at that time, see Ref. [38].*

Renewed interest in the M1 decay came from the collaboration between the Los Alamos (Lynn) and Oak Ridge (Raman) laboratories in the nineties. The observation of several M1 primary transitions with strength comparable to the E1 transitions led to the speculation that a mechanism analogous to the direct E1 capture may also be present for M1 primary decay in light nuclei. Lynn and Raman developed the theory that an orbiting neutron, in the field of the residual nucleus (the ground state of the target), makes a radiative transition to lower energy states. This theory, originally developed for the E1 capture, has been applied to the M1 data by replacing the E1 and M1 operators in the valence model, and generating the partial $\sigma_i(V)$ values. For the detailed formulation see Refs [11,30,40].

For the present analysis, a similar approach as the one used for E1 radiation has been qualitatively applied to M1 transitions. The results are given in Table 5 along with the appropriate cross-section parameters and the deduced total nonstatistical $\sigma_o(V)$ values.

TABLE 5. Results of σ(M1) contributions for light mass targets. All cross sections are given in barns, the σ(g)o values printed in red can have a strong resonant character.

Used notations:

σ_γ	thermal cross section taken from Ref. [31]
SIgE1,M1	total E1 and M1 strength extracted from capture data the PSF data base
ΣE1M1	total considered deexcitation of the capture state by E1 and M1 radiation
σ(M1)	total M1 strength ΣIgM1 converted in σ(M1)
σ(V)	total σ(M1) calculated as $\Sigma\sigma_i$ (V) values using the valence M1 model from Ref [17]
σ(V)*	^{29}Si from Ref. [35]
σ(V)**	a quote from Ref. [17]
M1Eg range	M1 transitions low and high energy in MeV
ρ(ng)(dp)	the correlation factor between the (n,g) IgEg^{-3} and (d,p) (2J+1)Sn from Refs [35, 38]

Nuclide		σγ [b]	ΣIγE1	ΣIγM1	ΣE1M1	σ(M1) [b]	σ(V) [b]	M1Eγ range MeV	ρ(ng)(dp)
Li	7	0.0445	1		1.00				
C	13	0.0039	0.998	0.16	1.16	0.0006		<1.8>	
	14	0.0015	0.925	0.074	1.00	0.00011	0.00930	1.3-2.1	
N	15	0.080	0.43	0.57	1.00	0.0456		0.8-5.6	
O	18	0.0005	0.99	0.01	1.00	0.00007		<2.7>	
F	20	0.0095	0.6	0.4	1.00	0.0038		0.3-6.6	-0.17
Ne	21	0.039	0.75	0.032	0.78	0.00125		4.0-6.8	
Na	24	0.525	0.42	0.59	1.01	0.3098		0.7-6.5	-0.06
Mg	25	0.0538	0.52	0.49	1.01	0.0264	0.00032	2.2-6.8	0.88
	26	0.199	0.2	0.84	1.04	0.1672	0.00022	3.9-11.1	
	27	0.0374	0.32	0.7	1.02	0.0262	0.0011	1.0-5.5	
Al	28	0.231	0.48	0.53	1.01	0.1224		0.5-7.7	0.93
Si	29	0.177	0.9	0.1	1.00	0.0177	0.130*	1.6-8.5	
	30	0.119	0.75	0.25	1.00	0.0298	Poor**	4.0-10.6	0.92
	31	0.107	0.98	0.02	1.00	0.0021	Poor**	4.3-6.6	
P	32	0.166	0.63	0.35	0.98	0.0581		1.2-8.0	0.84
S	33	0.518	0.94	0.069	1.01	0.0357		1.0-8.6	
	34	0.454	0.41	0.59	1.00	0.2679		5.3-11.4	
	35	0.256	0.92	0.04	0.96	0.0102		2.5-7	
	37	0.236	1		1.00				
Cl	36	43.6	0.49	0.45	0.94	19.62		2.0-8.6	1
	38	0.433	0.92		0.92			<4.2>	
Ar	41	0.66	0.99	0.01	1.00	0.0066		<5.4	
K	40	2.1	0.48	0.53	1.01	1.113		4-5.5	0.19
	41	38.8	0.63	0.29	0.92	11.252		1.9-8.8	
	42	1.46	0.79	0.15	0.94	0.219		1.6-6.1	
Ca	41	0.41	0.82	0.05	0.87	0.0205		3.4-6.4	
	43	0.68	0.99	0.01	1.00	0.0048		<6>	
	44	6.2	0.82	0.12	0.94	0.7496		6-7.8	
	45	0.88	0.45	0.55	1.00	0.4858		4.6-5.5	

	47	0.74	0.96	0.04	1.00	0.0326	<1.8>	
	49	1.09	1		1.00			
Sc	46	27.2	0.42	0.37	0.79	10.064	3.4-8.6	
Ti	49	8.32	0.98	0.02	1.00	0.1664	2.7-5.6	
	50	1.87	0.98	0.01	0.99	0.0187	3.5-6.5	
V	51	45	0.661	0.035	0.70	1.575	4.0-4.1	
	52	4.94	0.92	0.035	0.96	0.1729	1.6-5.6	
Cr	51	14.7	0.86		0.86		2.1-5	
	53	0.86	0.83		0.83		4.3-7.9	
	54	18.6	0.95	0.05	1.00		4.9-6.3	
Mn	56	13.36	0.82	0.18	1.00	2.4048	2.4-5.3	
Fe	57	2.59	0.48	0.53	1.01	1.3727	3.3-5.3	-0.08
	58	2.48	0.93		0.93			0.07
	59	1.32	0.89	0.03	0.92	0.0396	3.3-4.6	
Co	60	37.18	0.76	0.02	0.78	0.7436	2.6-5.1	-0.12
Ni	59	4.39	1.00	0.00	1.00	0.0044	<5.3>	
	60	73.7	0.78	0.01	0.79	0.7370	3.7-6.3	
	61	2.45	0.98	0.01	0.99	0.0213	3.6-4.1	
	63	14.9	0.78	0.12	0.90	1.8029	3.1-3.6	
	65	1.63	0.98	0.01	1.00	0.0217	2.8-3.8	
Cu	64	4.5	0.8	0.02	0.82	0.09	3.4-6.7	0.02
	66	2.17	0.72	0.09	0.81	0.1953	2.5-4.9	
Zn	65	0.731	0.95	0.05	1.00	0.0366	3.6-6.1	
	67	0.62	0.97		0.97			
	68	7.5	0.92	0.08	1.00	0.6	4.9-7.4	
	69	1.07	0.67	0.33	1.00	0.3531	3.9-4.4	

Several of the calculated σ(V) in Table 5 are negligibly small or rather controversial (such as ^{29}Si) and therefore, it is not possible to draw any conclusions on the M1 component. It is beyond the scope of this work to continue to speculate about possible reasons for these results, the only definitive statement that can be made is that the low-energy M1 component is present. As a graphical confirmation of the unexplained low-energy M1 behavior, two representative examples are shown in Fig. 8 for ^{24}Na and ^{28}Al nuclides as provided by S. Goriely. They show the thermal capture PSF from the THC database (2019) compared with the D1M + QRPA + 0lim and shell model calculations. The enhancement of the E1 strength above both theoretical values can be explained by the omission of the DC contributions in both calculations. On the other hand, the observed M1 enhancement may suggest that there must be another strength component contributing to the increasing PSF M1 strength in the zero-energy limit. A possible role of the scissor excitations or speculation about the parameters of the SF resonance (E_o(SF), Γ(SF) and its tail E_γ dependence) should be considered. Finally, an in-depth theoretical study of the non-statistical behavior of the M1 radiation is recommended.

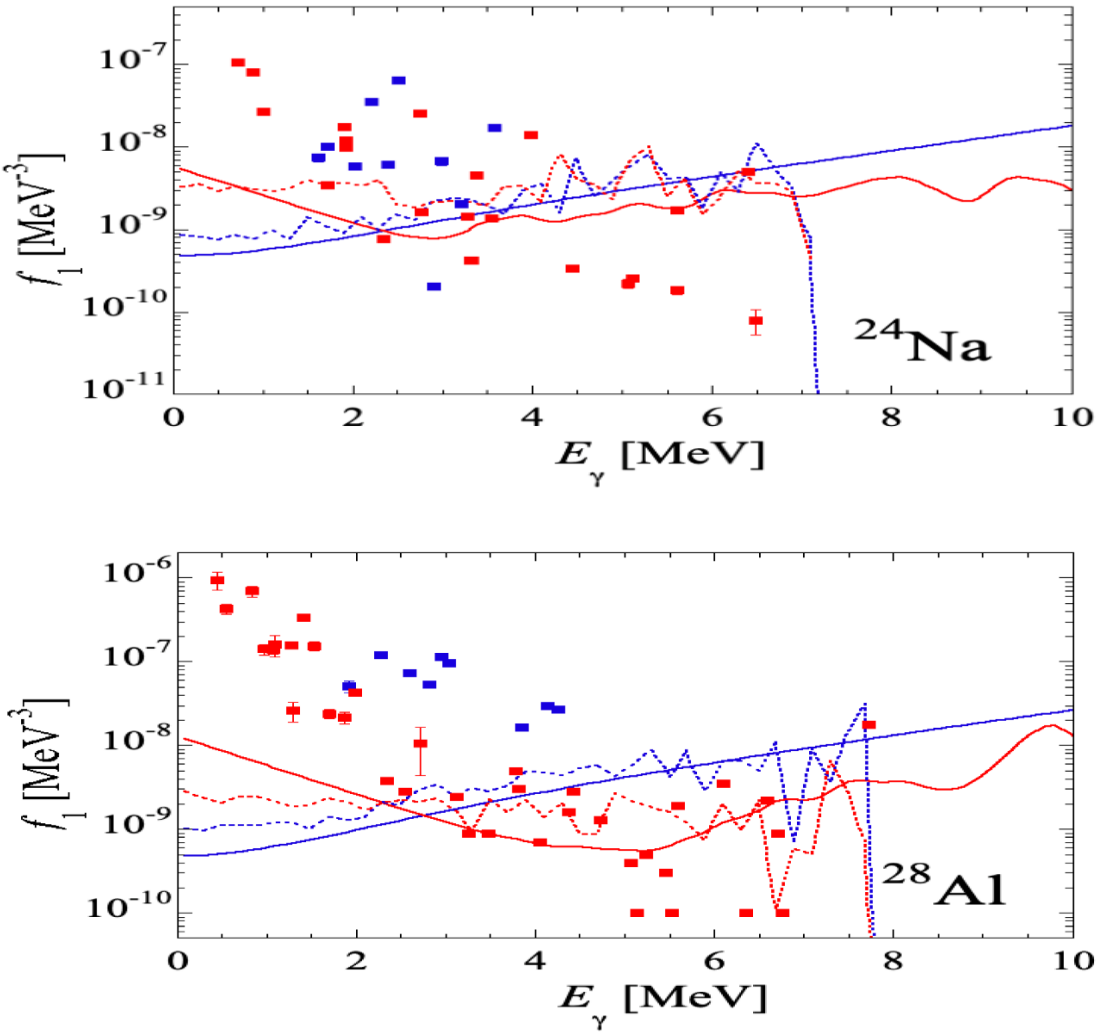

FIG. 8. *Comparison of the PSF evaluation of ^{24}Na and ^{28}Al with theoretical predictions. Both E1 and M1 data are in good agreement with predictions down to E_γ = 4MeV and from this energy a systematic increase of the strength takes place. The full curves are the results of the D1M + QRPA + 0lim calculations and the dotted curves originate from the shell model calculations [41]. The blue and red color is for E1 and M1 multipolarities, respectively. Note the remarkable agreement between the D1M + QRPA and SM calculations. The existence of the low-energy PSF enhancement, known from the seventies, is shown.*

M1 Conclusions: The presence of the M1 strength with increasing contribution as E_γ approaches zero has been verified experimentally for masses A < 70, especially below A ~ 45 (shown in Fig. 4). The D1M + QRPA + 0lim and shell model calculations predict an M1 strength significantly lower than the measured strength. The main observations are:

- A complete theoretical description of the total M1 strength valid in the whole energy region and for masses A < 70 is still missing. The statistical SF(M1) resonance model has been confirmed only for higher energies..
- The presence of the M1 enhancement at low energies is, however, related to the specific composition of the thermal capture state and, with increasing neutron energy, the statistical behavior of the CN becomes dominant. This means that the thermal capture PSF(M1) data may again, as with the PSF(E1) data, differ from the general PSF trend observed in nuclides with heavier masses that are dominated by statistical contributions.
- The E1/M1 strength ratio can be used to validate the upbend systematics (e.g. that of Goriely from Ref. [6]) in this mass range.

4. The ^{57}Fe neutron capture

The ^{57}Fe nucleus has been studied extensively using the different neutron-capture techniques and is therefore an excellent example to demonstrate the state of the art of thermal neutron capture data at the beginning of the 21st century. The ^{57}Fe nucleus belongs to the group of heavy nuclides with mass A < 70 for which the nonstatistical processes may still compete with the already sizeable statistical CN mode. The nucleus was studied in the charged-particle-gamma-coincidence experiment in 2004 [4] which was the primary OSLO experiment demonstrating the low energy PSF enhancement. It was also studied in detail as part of the PhD thesis of R. Vennink [42] in 1980. The author of the present report (JK) was the supervisor of the PhD work and hence, has the details of the experiment.

4.1. Thermal PSF data

The thermal capture data from the ECN Petten group were used in the previous PSF analysis [42] and recently, the 2017 data from the IKP/UJF collaboration [10] have also been included. It is therefore interesting to compare these two measurements to show the progress that has been achieved in more than two decades. The derived PSF data are shown in Fig. 9.

As a general observation, the improvements in the recent capture measurements performed in the available facilities – compared to the older capture data from the period 1960-1980 – are mainly related to the higher quality of the thermal beams, the gamma-ray detection technology, and data analysis tools, as well as to the absolute I_γ calibration and the decay scheme construction methods.

In the case of the ^{57}Fe ECN data, the thermal beam was a standard horizontal HFR beam filtered against the fast neutrons by quartz and bismuth crystals while the IKP reactor used the guided cold neutron beam with the sample placed at 30 m from the reactor in a background shielded area. The samples were natural Fe [42] compared to the highly enriched 99.94% ^{56}Fe sample used in [10]. This difference resulted in a decreased background and led to the improved detection sensitivity as shown in Table 6 that lists the number of transitions assigned to the ^{56}Fe(n,γ)^{57}Fe reaction in both experiments.

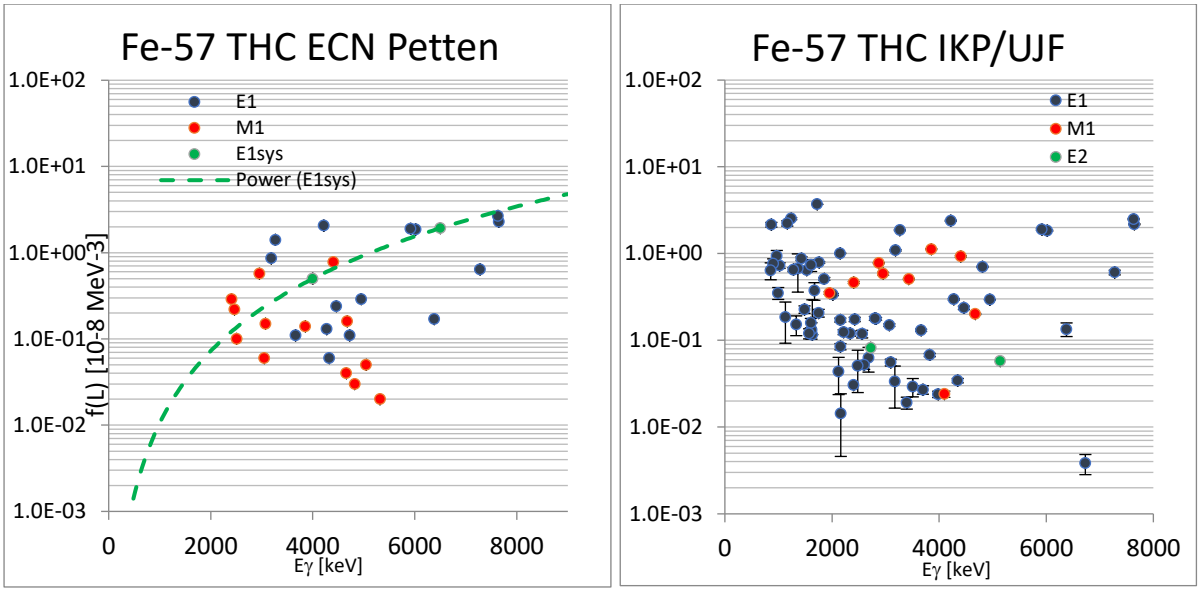

FIG. 9. *PSF ^{57}Fe thermal capture data from the ECN measurement [41], compared with the <<f(E1)>> 6.5 MeV systematics, given by the green dashed line, are in the left plot. The E1 data are in a good agreement with the systematic prediction even in the region E_γ = 2 - 5 MeV. The energy region covered by the data is from 2.4 MeV to 7.6 Me. The statistical errors are below 10%. The recent IKP/UJF data [10] are in the right plot and show many more data points, also including the E2 data with a much broader energy region from 0.8 to 7.6 MeV and a lower sensitivity cut off.*

TABLE 6. Number of observed g-transitions in two experiments from Refs [10,42]

Used notation:
#g, pg, sg, 'unasig' and total stand for ^{57}Fe assigned, primary, secondary, unassigned, and total number of transitions, respectively.

Lab	**Th beam**	**Target ^{56}Fe**	**# g**	**# pg**	**#sg**	**# unasig**	**#total**
ECN Petten	Filtered hor.	91.8%(nat)	191	33	158	62	253
IKP Budapest	Guided hor.	99.94%	453	88	365	19	472
UJF Rez	Filtered hor.	91.8%(nat)		88	~70%		

The number of assigned primary transitions is influenced by the different low-energy cut-off thresholds in these two measurements, 2.4 MeV and 0.8 MeV, respectively. Quite surprisingly, however, the summed intensities ΣI_γ (primary) in the energy window ΔE_γ = 2.8 – 7.6 MeV is almost the same in both cases, namely 96.6% and 94.4% for the ECN 33- and IKP 41 data, respectively. This agreement confirms the quality of the absolute I_γ normalization in both experiments. Furthermore, it proves that when the sum of primary intensities is above 90%, the dominant part of the decay strength has been exhausted. The 47 primary IKP transitions, having energies between 0.8 to 2.4 keV, contribute to only ΣI_γ = 2.3% of the total decay strength, and the majority remain unplaced in the ENSDF level scheme (i.e., they have no assigned levels).

One reason for the difference in assigned transitions in the two measurements is the procedure for assigning transition in the decay scheme. In the earlier analyses, the assignments were based primarily on E_γ and/or matching the sum of E_γ to the adopted level schemes in the ENSDF database with the aid of the Ritz combination principle. Such a procedure was used to obtain

the ECN data [42] as well as many earlier data, but there was an obvious limitation: it could not be applied when the nuclide level scheme was not available in ENSDF, and such fit was not possible. In the IKP/UJF experiment, for the first time, the sum γ–γ coincidence method has been used to verify the multipolarity assignment experimentally and subsequently propose the level. This is by far the most advanced implementation of the neutron capture technique, but unfortunately, the results have not been incorporated into the ENSDF database yet. The ENSDF dataset for ^{57}Fe has a literature cut-off 24-Sept-1998 and includes the data of [42] but not of [10].

We have used this exceptional new data [10] in our analysis for a preliminary comparison with other PSF evaluations as well as the analysis of Firestone [43] that is also based on the same (n,γ) data [10]. The results are shown in Fig. 10, with the left panel taken from Firestone [43] and the right panel displaying the present analysis (blue squares). Both binned (n,γ) primary data curves are in a relatively good agreement except for the lowest data point in Firestone's evaluation (green cross in the right panel). It represents the binned M1 data point at $\langle E_\gamma \rangle \sim 400$ keV which, however, disagrees with the lowest primary transition at $E_\gamma = 856$ keV and does not satisfy the conditions for assigning M1 multipolarity. All the transitions with $E_\gamma < 2$ MeV have no multipolarity assignments and are generally labeled only as dipole transitions. The PSF extracted from the thermal capture data [10] (blue squares) has an energy distribution that is in excellent agreement with the 2004 Oslo data (red circles), despite the factor of 2 difference in scale between both predictions. Such a factor of 2 difference in scale is probably due to uncertainties associated with the Oslo normalization procedure. The THC PSF also shows an upbend at energies below ~3 MeV. This comparison illustrates the power of THC experiments as they can provide reliable PSF information also at low energies.

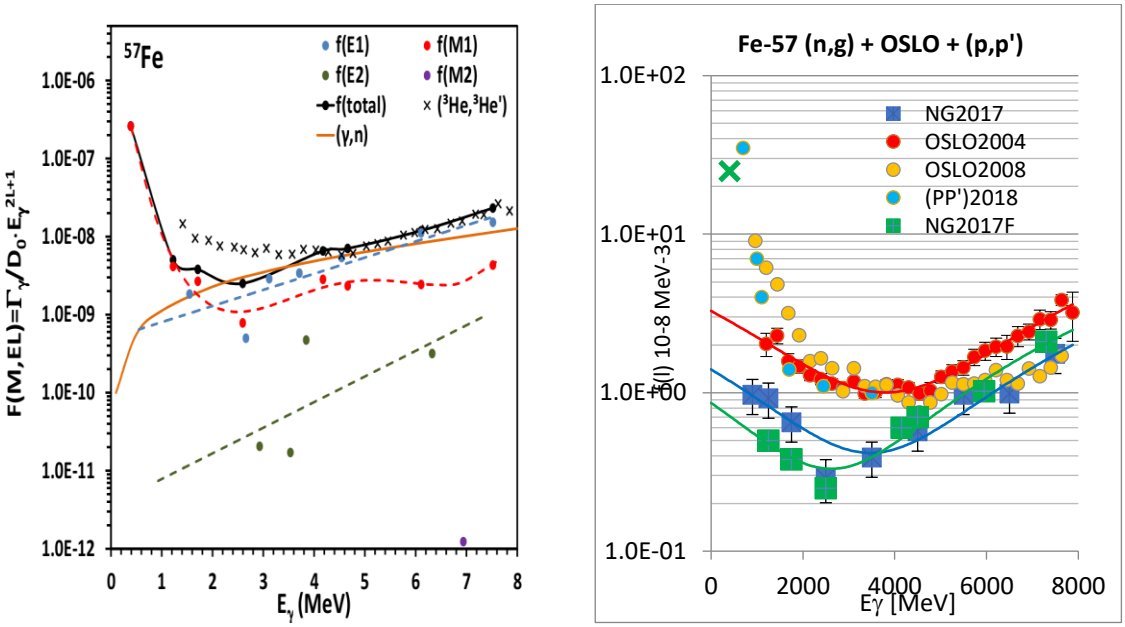

FIG. 10. *^{57}Fe PSF extracted from thermal capture data from the Budapest/Rez experiment [10] used in a preliminary comparison with other experimental PSF. The left panel is from Firestone [43]; it also includes data from the (^{3}He,^{3}He)^{57}Fe OSLO2004 experiment. The binned PSF data are in the right panel given as green squares; the green cross (2018F) is discussed in the text. The panel on the right compares the total dipole PSF from the present work (blue square) with all the OSLO data including the latest (p,p')^{56,57}Fe[44] ratio method E_x dependence prediction normalized to OSLO data at 3.5 MeV. Note the agreement between the binned Firestone and present evaluations (square data points).*

4.2. More on ^{57}Fe PSF

The presence of the 2p giant resonance in the light mass region means that for some nuclei, the DRC data can be used to compare the E1 and M1 modes of the same transition due to the parity switch, as found later in the ^{36}Cl nucleus [34]. The dominant single p-wave resonance is also present in the ^{56}Fe target at E_n = 1.167 keV with J = 1/2-. It has been measured at the BNL fast chopper in 1970 [45] and has been included as a source in the DRC database.

It is therefore useful to compare these two independent experiments, the thermal and resonance capture, for the absolute intensity calibration. In the THC measurement the calibration from the external calibration sources has been used to derive the absolute intensity as the number of gamma's/100 neutrons, while in the DRC measurement the partial radiative widths $\Gamma_{\gamma i}$ from the time-of-flight measurements have been applied. The comparison is shown in Fig. 11 and the similarity between these two spectra is very satisfactory.

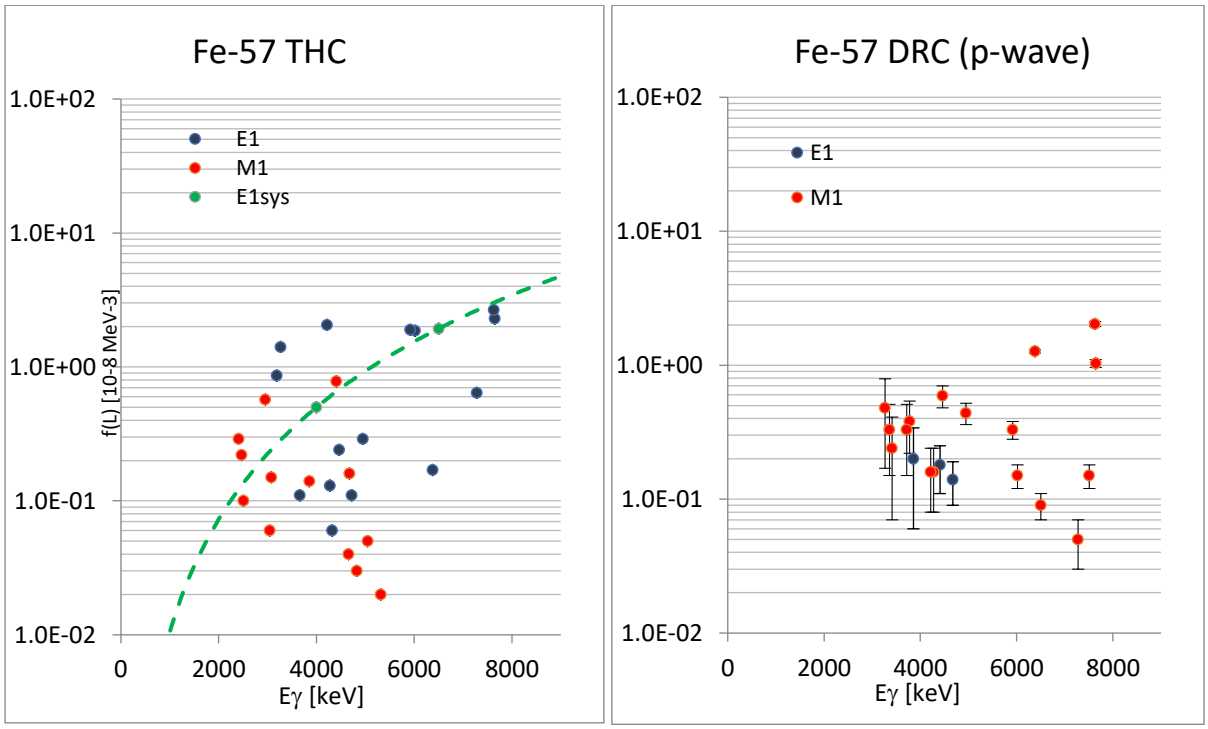

FIG. 11. *Comparison of the PSF thermal data ^{57}Fe with the discrete resonance capture from the p-wave resonance at En = 1.167 keV and J = 1/2-. The thermal E1 and M1 data switch their multipolarities in the p-wave capture and are in a reasonable agreement with each other considering the PT fluctuations. For the DRC PSF analysis the $\Gamma_{\gamma 1}$ and D_1 values from Ref. [31] have been used. Note a certain similarity in the high-energy transitions and increased statistical error of the DRC measurement.*

Particularly, the high-energy E1 and M1 transition intensities of both THC and p-wave DRC data agree very well, something that was also observed in the case of ^{36}Cl [34] and was attributed to a non-statistical influence, however, without any explanation. The plot of both data sets as the combined ^{57}Fe PSF (THC + DRC) entry is shown in Fig. 12.

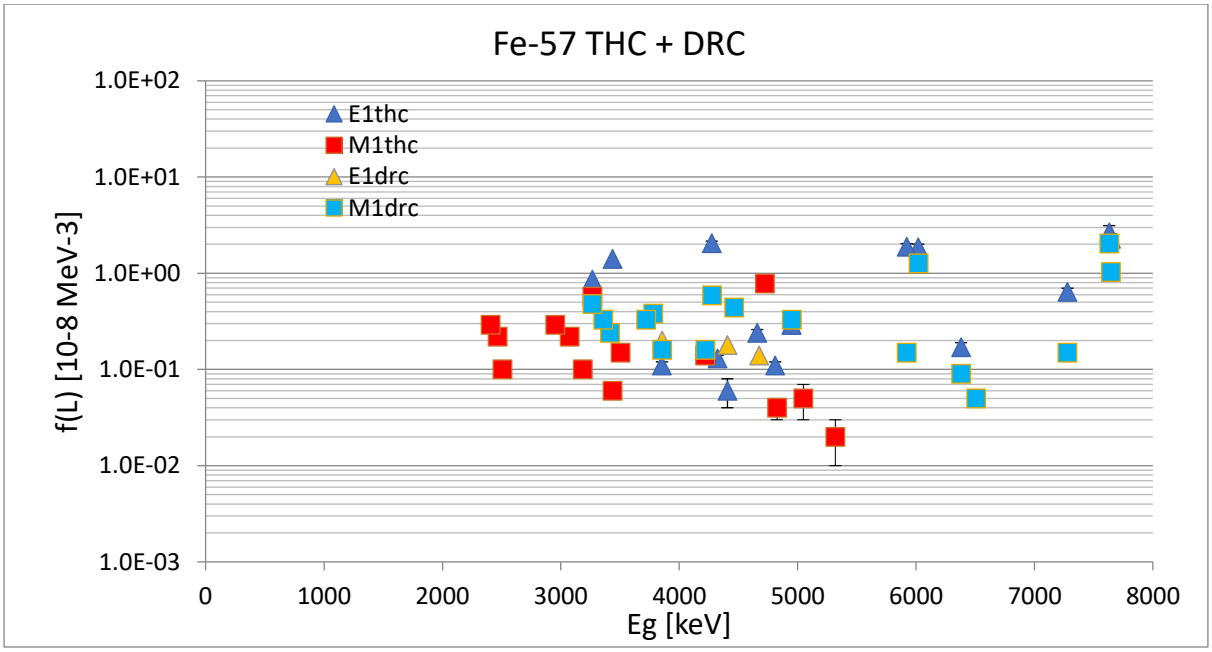

FIG. 12. *The combined thermal and resonance PSF data of the ^{57}Fe nuclide built from two independent experiments. Note a good agreement of both E1 (triangles data points) and M1 (squared data points) between these measurements and used absolute Iγ normalizations.*

Many thermal capture data have been compared with the D1M + QRPA + 0lim calculations in Refs [8,9,41] as a standard experiment vs. theory verification. The comparison for ^{57}Fe is shown in Fig. 13. Theoretical predictions agree reasonably well with experimental data for both E1 and M1 transitions. Note that below 2 MeV, no primary experimental data have been found in Ref. [42].

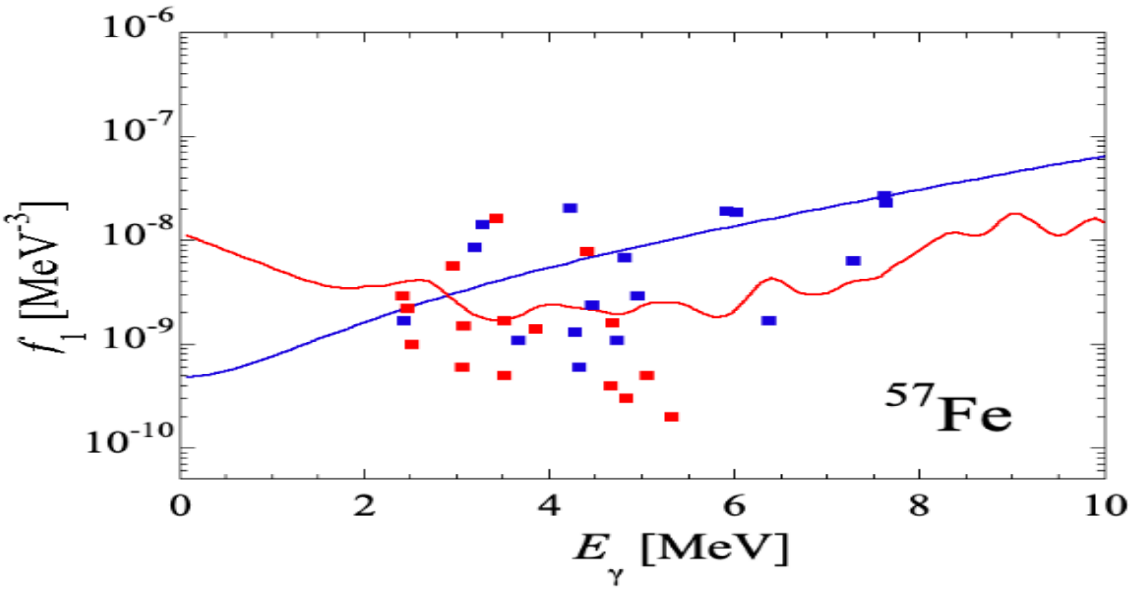

FIG. 13. *Comparison of the PSF evaluation of ^{57}Fe with the theoretical prediction. The M1 data are in good agreement with the prediction in the region E_γ = 2 - 5 MeV. The curves are the results of the D1M + QRPA +0lim calculations and the blue and red colors are for E1 and M1 multipolarities, respectively. Note a reasonable agreement between the calculations and E1 and M1 strengths.*

4.3. Recommendations for future work

1. There is a wealth of nuclides in the updated THC database, listed in Table 1, for which low energy transitions exist with known origin for both the primary and secondary transitions. In these cases, an extended analysis of the data may reveal useful information on the trend behavior as well as on the physics origin of the M1 strength (upbend, scissors mode, spin flip).
2. The completeness of the level scheme is essential for the PSF analysis and must be tested by calculating the quantities ΣI_γ(Primary), $\Sigma E_\gamma I_\gamma$/Bn, and ΣI_γ(Secondary to the ground state) which should be equal or close to one within their stated uncertainties.
3. The data mentioned in item #1, which include not only primary transitions but also high-quality secondary transitions, have not been used to date to analyze capture data and extract PSF. These data, with their solid decay scheme assignments and excellent intensity balances for the observed transitions (I_γ (in)/I_γ(out) ratios close to one), could be used in a similar data analysis as the one adopted by the Oslo method. In other words, the bound levels could be treated as entry capture states and the secondary transitions could be treated as 'primary' transitions below the neutron binding energy. We have tested this approach on the ^{57}Fe ECN data and the reduced intensity IR = I_γ/E_γ^3 of primary and secondary transitions is shown in Fig. 14.

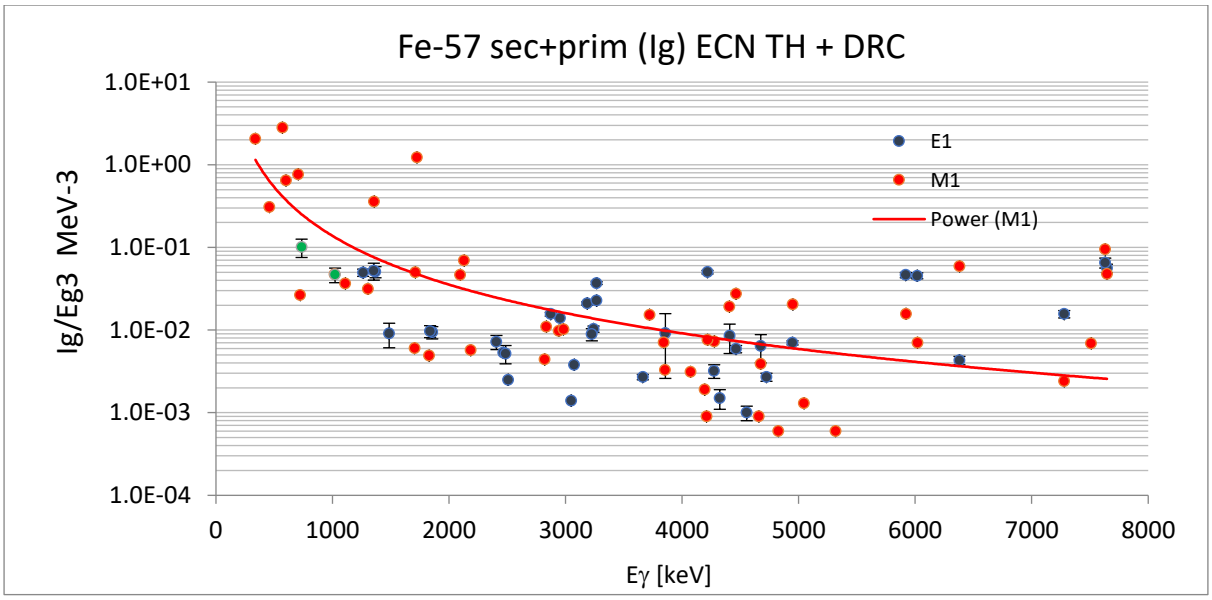

FIG. 14. *The combined primary and secondary data from different initial states of one experiment from [42]. The B_n capture state and six bound levels at E_i = 750, 1725, 2836, 3240, 4210 and 4692 keV have been used. The main advantage is that for the secondary transitions all spin/parity values are known allowing us to keep the E1 and M1 assignments. Note the smooth overlap of both data sets between 2 – 4 MeV. The plotted M1 curve serves only as a trend of the E_γ dependence.*

4. There is a similarity between the secondary transitions approach and OSLO measurements, which also uses the binned bound levels < B_n as initial states of the decay, however, further work is required to convert the relative intensities IR into PSF data, which could be achieved by empirically deducing the bound level Γ_γ (from the half-lives) and the spacing D (from the cumulative plot of discrete levels). At this moment we are testing the empirical Γ_γ and D inputs and the preliminary results are shown in Figs 15 and 16.

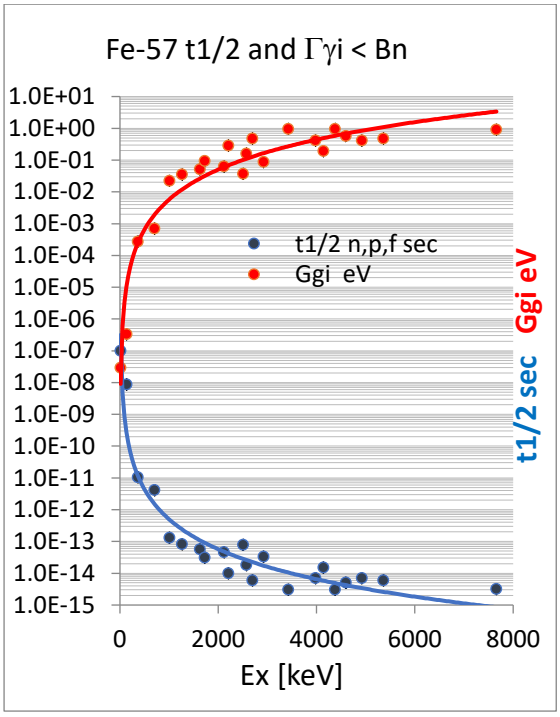

FIG. 15. *Plot of the bound state $t_{1/2}$ and $\Gamma\gamma_i$ parameters for the ^{57}Fe nucleus as a function of excitation energy in ^{57F}e. States with J=1/2, 3/2 and 5/2 spins have only been considered because of the dipole dominance of transitions. The thermal f -state half-life has been extracted from the $<\Gamma\gamma>$ = 0.9 eV value from the resonance region. Note the dramatic change of both parameters in the < 1.5 MeV region.*

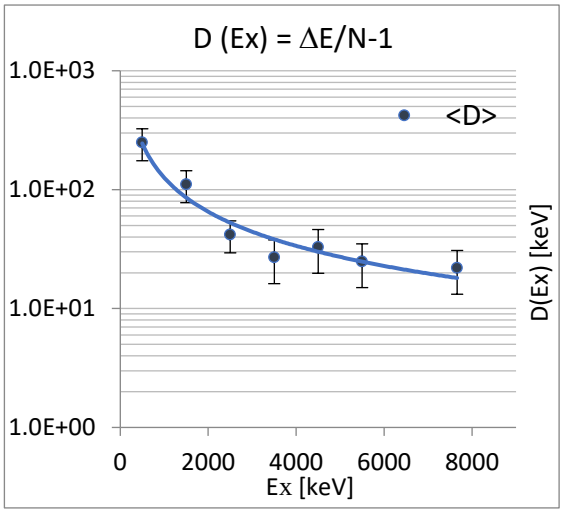

FIG. 16. *The average spacing values estimated from the cumulative discrete levels plot between 0 and 5 MeV from ENSDF database and extracted for $D(E_x)$ = 1 MeV broad regions. The fitted curve is the power trend curve and the associated error bars below 5 MeV have been estimated to be about 20%. The data up to ~4 MeV include all spins and parities.*

5. The use of the secondary transitions allows us to compare the 0lim PSF data extracted from the primary transitions from states close to the B_n with those from secondary transitions between states close to the ground state.
6. The E1 strength is composed of two independent contributions, the DC and the statistical CN contribution. The estimated integral DC contribution in the case of ^{57}Fe amounts to78% of the total E1 strength (see Table 3).
7. Since the TALYS code now includes the DC model, DC contributions can be calculated and used to test the 50-year-old integral data of Mughabghab.

5. Summary – perspectives

The thermal neutron capture data of low mass A < 70 nuclides have been revisited, improved, and incorporated into an upgraded NDS PSF database. The available information on the direct capture (DC) mode has been surveyed and DC contributions to the total E1 and M1 primary strength established.

Looking into the future, we consider the following projects worth pursuing:

Primary data

The achieved improvements in recent thermal neutron capture measurements have been acknowledged and tested in detail for ^{57}Fe. The main improved feature is the extension of the low energy E_γ detection limit close to zero energy. The primary transitions, assigned with the help of stronger arguments and reliably determined decay schemes, allow us to probe the "upbend" region directly and not indirectly, by means of the shape trend analysis, as in many earlier attempts. The candidate nuclides for possible reanalysis are listed at the end of Section 2. The preliminary comparison between different PSF experimental data for ^{57}Fe (see Fig. 10) suggests the need to re-analyze many low energy PSF data with the THC high quality data.

Secondary data

The wealth of secondary transitions, assigned with the same accuracy as the primaries, offer the possibility to study the PSF data using the decay of bound levels with E_x < Bn. This is a novel approach, which allows to study the PSF behavior not only for the E_γ dependence but also as a function of the initial state with E_x energy in the decay scheme. This approach is currently being tested.

M1 strength

The enhancement of low-energy M1 transitions is confirmed. Because the single-particle transitions s1/2 -> s1/2 and s1/2 -> d3/2 are forbidden, the semi-direct processes may be the main source of non-statistical effects influencing the CN giant M1 SF resonance.

Finally, extensive calculations of the E1 DC component using the TALYS code would shed light on decades old integral data.

Acknowledgement

The author should like to thank the IAEA NDS for initiating and supporting this work and for help and advice, with figures from Stephane Goriely and many useful comments from Robin Forrest and Frank Becvar.

References

[1] S. Goriely, et al., Eur. Phys. J. A **55** (2019) 172.
[2] S. Goriely and V. Plujko, Phys. Rev. C**99** (2019) 014303.
[3] S. Goriely, et al., Phys. Rev. C**94** (2016) 044306.
[4] A. Voinov, et al., Phys. Rev. Lett. **93** (2004) 142504.
[5] M. Guttormsen, et al., Phys. Rev. C **71** (2005) 044307.
[6] S. Goriely, et al., Phys. Rev. C**98** (2018) 014327.
[7] J. Kopecky and F. Becvar, Comparison of Photon Strength Functions from the OSLO Method with Neutron Capture Systematics, IAEA report INDC(NDS)-0868, 2022, https://www-nds.iaea.org/publications/indc/indc-nds-0868/
[8] J. Kopecky, Photon Strength Functions in Thermal Capture, IAEA report INDC(NDS)-0799, 2020, https://www-nds.iaea.org/publications/indc/indc-nds-0799/
[9] J. Kopecky, Photon Strength Functions in Thermal Capture II, IAEA report INDC(NDS)-0815, 2020, https://www-nds.iaea.org/publications/indc/indc-nds-0815/
[10] R. Firestone, et al., Phys.Rev. C**95** (2017) 014328.
[11] J. Lynn, et al., Phys. Rev. C**44** (1991) 764.
[12] S.F. Mughabghab, et al. Phys. Rev. C **26** (1982) 2698.
[13] E.T. Jurney, et al. Phys. Rev. C **56** (1997) 118.
[14] W.V. Prestwich, et al. Z.Phys. A **325** (1986) 321.
[15] J. Tomandl, et al., Phys. Rev. C **69** (2004) 014312.
[16] T.A.Walkiewicz, et al., Phys. Rev. C **45** (1992) 1597.
[17] S. Raman, et al., Phys. Rev. C **46** (1992) 972.
[18] S. Raman, et al., Phys. Rev. C **32** (1985) 18.
[19] S. Raman, et al., Phys. Rev. C **30** (1984) 26.
[20] J.F.A.G. Ruyl, et al., Nucl. Phys. A **419** (1984) 439.
[21] J. Kopecky, et al., Nucl. Phys. A **188** (1972) 535.
[22] S. Raman, et al., Phys. Rev. C **70** (2004) 044318.
[23] A.M. Lane and J.E. Lynn, Nucl. Phys. **17** (1960) 563 and 586.
[24] A.M.J. Spits and J.A. Akkermans, Nucl. Phys. A **215** (1973) 260.
[25] A. Koning, et al., TALYS: Modeling of nuclear reactions, Eur. Phys. J. A **59** (2023) 131.
[26] J. Kopecky, A.M.J. Spits, Some features of the correlation between the (d,p) and (n,g) reduced width, RCN report 1974, RCN-74-055.
[27] J. Kopecky and C. Plug, Tables of the (n,g) (d,p) correlations in the 3s- region" RCN Report 1975, RCN-75-005.
[28] J. Kopecky, A.M.J. Spits, A.M. Lane, Phys. Lett. B **49** (1974) 323.
[29] S. Mughabghab, Non-statistical effects in neutron capture, III Int. School on Neutron Physics, Alusha (The Crimea) USSR, April 1978.
[30] J.E. Lynn and S. Raman, in: Capture Gamma-ray Spectroscopy, 14-19 Oct 1990, Pacific Grove, CA, AIP Conf. Proc. **238** (AIP, New York, 1991) p. 555. https://doi.org/10.1063/1.41220
[31] S.F. Mughabghab "*Atlas of Neutron Resonances*" (Elsevier 2018).
[32] A. Bohr and B. Mottelson, "Nuclear Structure Vol. II", (Benjamin, London) 1975.
[33] J. Kopecky, Anomalous M1-capture in mass region A=20-40, Proc. Int. Conf. on the Interactions of Neutrons with Nuclei, Lowell, Massachusetts, USA, July 6-9, 1976, (CONF-760715-P2) p. 1285. Web. https://www.osti.gov/biblio/7236382.
[34] R.E. Chrien, J. Kopecky, Phys. Rev. Lett. **39** (1977) 911.
[35] C.F. Clement, A.M. Lane, J. Kopecky, Phys. Lett. B **71** (1977) 10.
[36] G.E. Brown, Nucl. Phys. **57** (1964) 339.
[37] A.M. Lane, Inv. Paper at Conf. on Statistical Properties of Nuclei, Hvar, Yugoslavia, October 1 (1979).

[38] J. Kopecky, Mass and energy dependence of radiative strength near neutron threshold, Proc. Int. Conf. on Nuclear Physics, Berkeley, Cal., USA., August 24-30, 1980. Nucl. Phys. A 354 (1981) 1-2 in Abstracts.
[39] J. Kopecky, Nonstatistical features of M1 transitions near neutron threshold, ibid, p. 209.
[40] S. Raman, et al., Phys. Rev. C **41** (1990) 458.
[41] S. Goriely, P. Dimitriou, et al., Reference Database for Photon Strength Functions, Eur. Phys. J. A **55**:172 (2019), and S. Goriely and K. Sieja, private communication.
[42] R. Vennink et al., Nucl. Phys. A **344** (1980) 421.
[43] R. Firestone, *Presentation to the3rd RCM of the Coordinated Research Project on Photonuclear Data and Photon Strength Functions*, IAEA NDS (Vienna) 2018 and https://www-nds.iaea.org/publications/indc/indc-nds-0745/
[44] M.D. Jones, et al., PHYS. Rev. C**97** (2018) 024327.
[45] R. E. Chrien, et al., Phys. Rev. C **1** (1970) 973.

Nuclear Data Section
International Atomic Energy Agency
Vienna International Centre, P.O. Box 100
A-1400 Vienna, Austria

E-mail: nds.contact-point@iaea.org
Fax: (43-1) 26007
Telephone: (43-1) 2600 21725
Web: http://nds.iaea.org